DISPLACEMENT-BASED MEASUREMENT OF STATIC AND DYNAMIC COEFFICIENTS OF FRICTION

Christian T. Lomascolo, John Ziegert, and Tony L. Schmitz
Department of Mechanical Engineering and Engineering Science
University of North Carolina at Charlotte
Charlotte, NC

INTRODUCTION

Experimental methods are commonly used to identify friction behavior, particularly for manufacturing processes [1-22]. The majority of these friction measurements are made on tribometers, which apply a normal force to a pin that is pressed against a rotating or translating surface. The normal and friction forces are measured and the friction coefficient is calculated. However, misalignment between the force transducer axes and the motion and the applied direction of the normal force are critical factors in establishing the accuracy of the derived coefficients of friction [23].

Current methods used to measure friction behavior and parameterize complex friction models can suffer from high uncertainty, especially for low friction interfaces. Relative uncertainties on the order of two to four parts in 10^2 of the measured value are typical for low friction interfaces [23]. In contrast, displacement can be measured by laser interferometry with relative uncertainties on the order of a few parts in 10^7, four to five orders of magnitude better. The research described in this paper will evaluate a fundamentally new method for measuring friction and parameterizing friction models with lower uncertainty than conventional methods. The innovation is the use of high-accuracy displacement and velocity measurements during dynamic motions to characterize the energy dissipation.

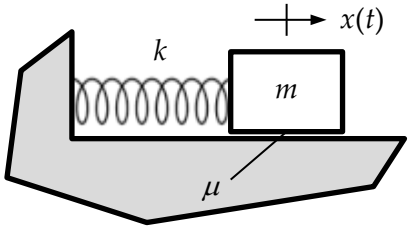

Figure 1. Spring-mass oscillator with Coulomb friction.

MEASUREMENT THEORY

To find the coefficient of friction between two materials, a normal force is applied between them and relative motion is provided. As shown in Fig. 1, the moving mass, m, is given an initial displacement and decaying oscillating motion occurs due to the linear spring, k, and Coulomb (frictional) damping, μ. Given an initial displacement of the moving mass, a final displacement is obtained. In the proposed instrument, displacement is recorded using displacement measuring interferometry.

SIMULATION RESULTS

Sliding, or Coulomb, friction can be incorporated into the equation of motion describing the time-dependent displacement, $x(t)$, of the Fig. 1 spring-mass system as shown in Eq. 1. In this equation, F_f is the friction force (i.e., the product of the friction coefficient, μ, and the normal force, $N = mg$).

$$\begin{matrix} m\ddot{x} + kx + F_f = 0, \dot{x} > 0 \\ m\ddot{x} + kx = 0, \dot{x} = 0 \\ m\ddot{x} + kx - F_f = 0, \dot{x} < 0 \end{matrix} \quad (1)$$

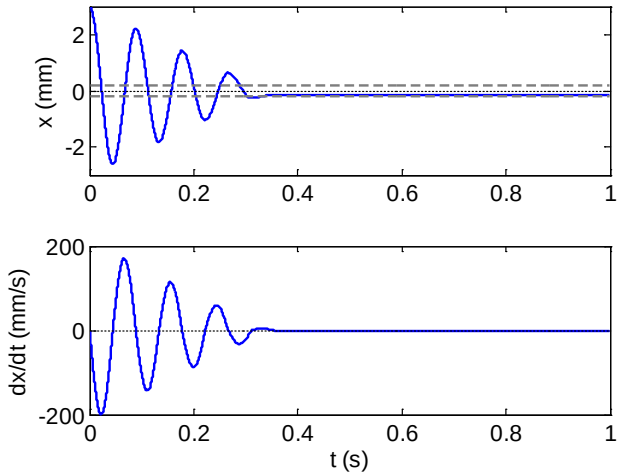

Figure 2: Free vibration result for x_0 = 3 mm.

Because the friction force always opposes the velocity direction, it is discontinuous. This yields the nonlinear second order, homogeneous differential equation shown in Eq. 1. For the displacement-based approach to be used in this research, the desired information is $x(t)$ (as well as its time derivative, or velocity). The relationship between the initial mass

displacement, $x(0) = x_0$, and the corresponding motion will be established. Specifically, due to the friction force, the final displacement, x_f, depends on x_0.

Consider the case where μ = 0.1, m = 1 kg, and k = 5×10^3 N/m for the model in Fig. 1. The free vibration response for x_0 = 3 mm (zero initial velocity) is displayed in Fig. 2, where x_f = –0.139 mm. It is observed that when the velocity reaches zero (lower panel near 0.1 s), if the current displacement is between $x_{lim} = \frac{F_f}{k} = \frac{\mu N}{k}$ and $-x_{lim}$, the motion stops. This limiting displacement (marked by the horizontal dashed lines in the top panel of Fig. 2) is the x value where the spring force is equal to the friction force. For a new initial displacement of x_0 = 1 mm, the final mass position is x_f = 0.176 mm; see Fig. 3.

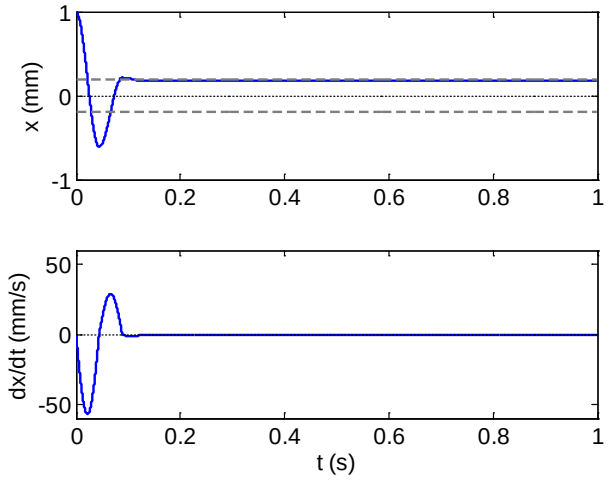

Figure 3: Free vibration result for x_0 = 1 mm.

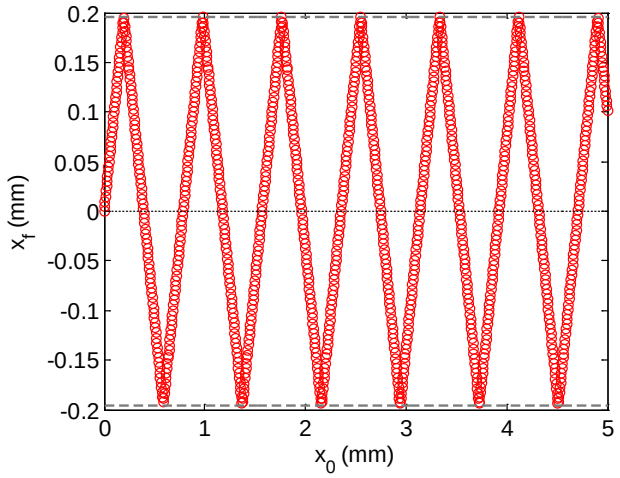

Figure 4: Initial vs. final displacement (Coulomb friction).

If the final displacement is plotted versus the initial displacement for this system, a periodic structure is revealed. This result is presented in Fig. 4. The period of the triangular waveform is $\frac{4F_f}{k} = \frac{4\mu N}{k}$ and its amplitude is x_{lim}.

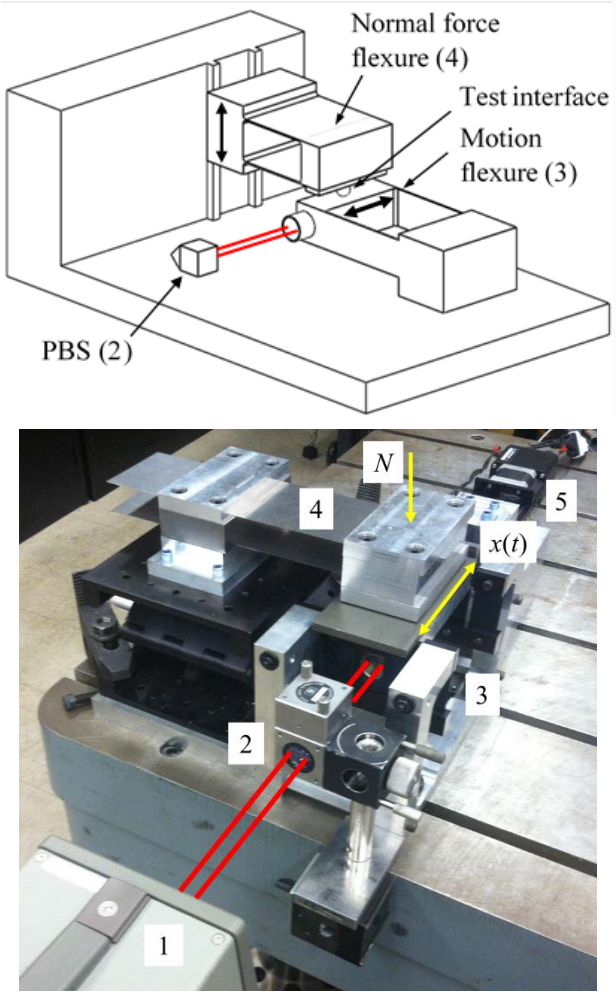

Figure 5: Schematic (top) and photograph (bottom) of prototype setup including: (1) DMI; (2) PBS; (3) motion flexure; (4) normal force flexure; (5) motor/stage/electro-magnet for initial displacement.

INITIAL EXPERIMENTAL RESULTS

To provide preliminary test data, a prototype setup was designed and constructed. The design concept used flexures for both the normal force application and the free vibration motion direction. Flexures were chosen to constrain the motion (ideally) to a single direction with low stiffness and a selectable natural frequency [24]. The setup is displayed in Fig. 5. The primary components were:

- displacement measuring interferometer (DMI) to measure the motion flexure displacement, x_0 and

$x(t)$; the DMI includes the laser head, polarizing beam splitter (PBS), and retroreflector (attached to the underside of the flexure in the Fig. 5 photograph)

- motion flexure – this provides the relative motion between the sample and counterface
- normal force flexure – this flexure was used to provide the prescribed normal force, N, between the contact surfaces (it is very stiff in the x direction, but flexible in the vertical direction); masses were stacked on the flexure to change the normal force
- motor/stage/electro-magnet for initial displacement – the electromagnet was energized to pull the flexure away from its equilibrium position to the prescribed initial displacement and then turned off to release the flexure and initiate free vibration.

The flexure dynamics were measured by impact testing, where an instrumented hammer is used to excite the structure and a linear transducer is used to record the corresponding motion [25]. This time domain data is converted to the frequency domain and the displacement-to-force ratio is calculated. This frequency response function can then be fit using modal analysis techniques to identify the natural frequency, stiffness, and damping ratio. In this case, the flexure had a dominant natural frequency of 12.6 Hz with a stiffness of 2574 N/m and a low viscous damping ratio of 0.0027 (0.27%).

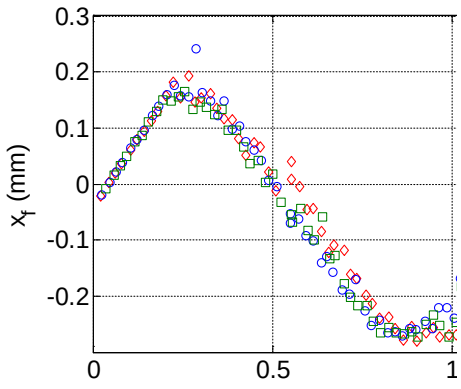

Figure 6: Initial vs. final displacement for UHMWP on anodized aluminum (three repeated trials).

In a first series of tests, the normal force between a flat pin (ultra-high molecular weight polyethylene, UHMWP, with a small percentage of polytetra-fluoroethylene, PTFE, added) and an anodized aluminum counterface was set to be 9.66 N, initial displacements of 0.025 mm to 1.0 mm were imposed, and the final displacement was identified from the free oscillation response measured by the DMI. The results of three repeated trials are presented in Fig. 6, where the horizontal axis is the initial displacement for the motion flexure mass/counterface and the vertical axis is its final displacement after oscillation. The triangular waveform shown in Fig. 4 was observed, so these promising initial results warrant further investigation.

In a second series of tests, rolling friction was examined by inserting a 4.76 mm diameter steel sphere between the UHMWP and anodized aluminum surfaces. Figure 7 shows a comparison of the free vibration for a 2 mm initial displacement with contact (sphere inserted with a normal force of 10.89 N) and no contact (flexure motion only). This increased energy dissipation due to friction is observed and demonstrates that this setup (or a modification) can be used for low friction interfaces.

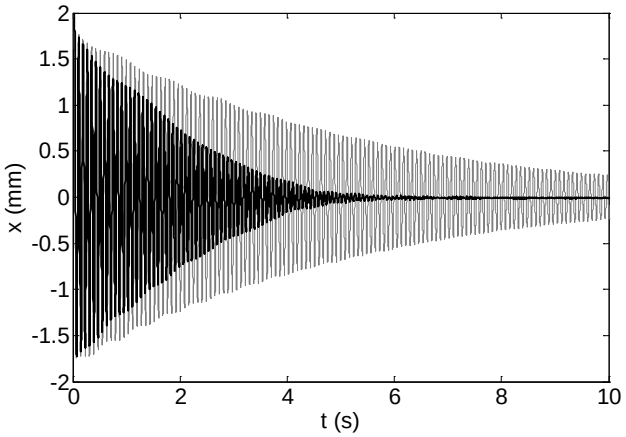

Figure 7: Free vibration for (gray) flexure only; and (black) rolling steel sphere between UHWMP and aluminum.

NEW DESIGN

A number of design improvements are planned for the new friction measuring machine:

- increase the motion flexure leaf spring length to decrease parasitic motions and reduce structural damping
- place the intersection of the measurement, pin/counterface contact, and force lines at the center of the flexure body to eliminate moments and Abbé error
- replace the normal force flexure with an air bearing
- use a large angle plate as the motion flexure mount.

A model of the new design is displayed in Fig. 8, where the angle plate supports the (vertical) force application to the pin using an air bearing and the base of the four flexure leaf springs that provide

(horizontal) linear motion of the motion platform (counterface). In operation, the motor will extend the stage that supports the electro-magnet (through a decoupling flexure) toward the motion platform. The electro-magnet will be energized to capture the motion platform. The motor will then retract the stage to provide the initial displacement of the motion platform (though leaf spring deflection). By de-energizing the electro-magnet, the motion platform will be released and will oscillate in the horizontal plane. The DMI will be used to measure the initial, time-dependent, and final platform displacements (the moving retroreflector will be attached to the motion platform; the DMI measurement axis will pass through the pin-counterface contact point to eliminate Abbé effects). The normal force will be varied by changing the deadweight mass on top of the cylinder that passes vertically through the (fixed) air bearing. The pin will be mounted on the bottom of this cylinder. The (vertical) normal force will press the pin against the counterface, which will be attached to the motion platform.

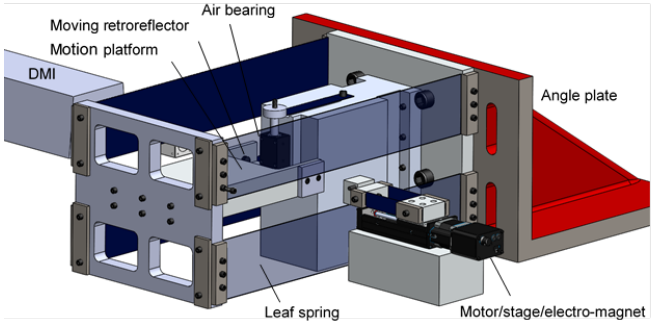

Figure 8: New friction measuring machine design.

DATA EVALUATION

A primary objective of this research is to enable friction model parameterization with increased accuracy. Therefore, the data evaluation will include the selected friction model, the measured displacement and velocity, and the friction measuring machine structural dynamics. The friction model will describe the friction force acting between the pin and counterface and will appear in the second order differential equation that describes the flexure motion:

$$m\ddot{x} + c\dot{x} + kx + F_f sgn(\dot{x}) = 0, \qquad (2)$$

where *c* is the viscous damping coefficient (due to the structural energy dissipation) and the signum function captures the velocity sign dependence of the friction force. To assign values to the friction model coefficients, the measured displacements (initial, time dependent, and final) will be compared to the solution of Eq. 2. This comparison can take several forms.

- An over-constrained optimization approach can be applied to identify the best-fit friction model parameters by minimizing the difference between the measured displacement and $x(t)$ and the Eq. 2 solution. The friction model can be identified from a single initial displacement by this technique. Multiple initial displacements will be used to verify consistent results.
- The global initial vs. final displacement behavior shown in Figs. 4 and 6 can be used to parameterize the friction model. In one scenario, multiple experiments will be used to determine {initial displacement, final displacement} pairs and the optimization problem will minimize the difference between these pairs and the corresponding Eq. 2 solution pairs. In other words, the friction parameters will be selected to achieve a best-fit between the simulated plot (Fig. 4) and its experimental counterpart (Fig. 6). In a second approach, the period and amplitude of the experimental initial vs. final displacement graph will be used to define the friction model parameters.
- The DMI provides high accuracy measurement of the instantaneous position and velocity of the moving counterface. Since the total energy in the system is the sum of the kinetic energy in the moving mass ($\frac{1}{2}mv^2$) and the potential energy stored in the flexure springs ($\frac{1}{2}kx^2$), it will be possible to track the instantaneous rate of energy dissipation in the system. When the viscous (and windage) losses are subtracted using data from free vibration of the system with no frictional contact, it will be possible to map the instantaneous rate of frictional energy dissipation over the entire experiment. This will enable an accurate quantification of variations in the frictional force over the full range of sliding velocities, including behavior near zero velocity. Simulated energy dissipation results are presented in Fig. 9 for μ = 0.01, m = 1 kg, k = 5×10^3 N/m, a 1% viscous damping ratio, and x_0 = 3 mm. As seen in the top panel, for no damping or friction, the energy is constant. The energy loss is exponential for viscous damping only and parabolic for friction only. It is a combination when both are present. In the bottom panel, it is observed that the energy dissipation rate increases from none to friction only to damping only to both and varies with velocity. The friction energy rate, FER in the figure, will be identified by subtracting the damping energy rate (measured with no friction contact) from the combined

energy rate. The friction force will be determined by dividing FER by the sliding velocity.

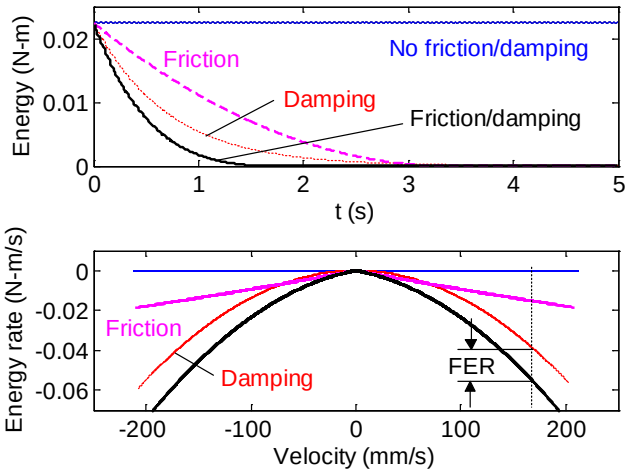

Figure 9: (Top) Energy loss vs. time; (bottom) energy loss per unit time vs. sliding velocity.

CONCLUSIONS

The goal of this research is to increase friction measurement accuracy with a particular emphasis on low friction applications. This will enable: improved modeling, prediction, and control of manufacturing processes; creation and evaluation of new manufacturing coatings and lubricants; and design of new low friction elements, including bearings of all types, to be used in manufacturing machines. To realize this goal, a novel displacement-based, dynamic measurement approach is being tested. This offers a new Lagrangian strategy with a focus on energy dissipation, as opposed to the traditional force-based Newtonian method for current tribometers.

This paper presented both simulated and experimental results to demonstrate the efficacy of the new displacement-based measurement strategy. A new friction measuring machine design was presented. Once it is constructed, new measurement results will be presented and the measurement uncertainty will be evaluated.

REFERENCES

[1] Kalpakjian, S. and Schmid, S., 2008, Manufacturing Processes for Engineering Materials, 5th Ed., Prentice Hall, Upper Saddle River, NJ.

[2] Astakhov, V., 2006, Tribology of Metal Cutting, Elsevier Science and Technology, Oxford, UK.

[3] Astakhov, V., 1998, Metal Cutting Mechanics, CRC Press, Boca Raton, FL.

[4] Tlusty, G., 1999, Manufacturing Processes and Equipment, Prentice Hall, Upper Saddle River, NJ.

[5] Yang, X. and Liu, C.R., 2002, A new stress-based model of friction behavior in machining and its significant impact on residual stresses computed by finite element method, International Journal of Mechanical Sciences, 44: 703-723.

[6] Olsson, H., Åström, K.J., Canudas de Wit, C., Gäfvert, M., and Lischinsky, P., 1998, Friction models and friction compensation, European Journal of Control, 4/3: 176-195.

[7] Armstrong-Helouvry, B., 1991, Control of Machines with Friction, Boston, MA, Kluwer.

[8] Armstrong-Helouvry, B., Dupont, P., and Canudas de Wit, C., 1994, A survey of models, analysis tools and compensation methods for the control of machines with friction, Automatica, 30/7: 1083-1138.

[9] Berger, E.J., 2002, Friction modeling for dynamic system simulation, Applied Mechanics Reviews, 55/6: 535-577.

[10] Hsu, S, Ying, C., and Fei Z., 2014, The nature of friction: A critical assessment, Friction, 2/1: 1-26.

[11] Barahanov, N. and Ortega, R. , 2000, Necessary and sufficient conditions for passivity of the LuGre friction model, IEEE Transactions on Automatic Control, 45/4: 830-832.

[12] Bliman, P.A. and Sorine, M., 1995, Easy-to-use realistic dry friction models for automatic control, Proceedings of the 3rd European Control Conference, ECC'95, Rome, Italy, pp. 3788-3794.

[13] Canudas de Wit, C., Olsson, H., Astrom, K.J., and Lischinsky, P., 1995, A new model for control of systems with friction, IEEE Transactions Automatic Control, 40: 419-425.

[14] Dahl, P., 1968, A solid friction model, The Aerospace Corporation, El Segundo, CA, Tech. Rep. TOR-0158(3107-18).

[15] Dupont, P., Hayward, V., Armstrong, B., and Altpeter, F., 2002, Single state elastoplastic friction models, IEEE Transactions Automatic Control, 47: 683-687.

[16] Ferretti, G., Magnani, G., Martucci, G., Rocco, P., and Stampacchia, V., 2003, Friction model validation in sliding and presliding regimes with high resolution encoders, Experimental Robotics VIII, B. Siciliano and P. Dario, Eds. New York: Springer-Verlag, pp. 328-337.

[17] Ferretti, G., Magnani, G., and Rocco, P., 2004, Single and multistate integral friction models, IEEE Transactions Automatic Control, 49: 2292-2297.

[18] Lampaert, V., Swevers, J., and Al-Bender, F., 2002, Modification of the Leuven integrated

friction model structure, IEEE Transactions on Automatic Control, 47/4: 683-687.
[19] Swevers, J., Al-Bender, F., Ganseman, C.G., and Prajogo, T., 2000, An integrated friction model structure with improved presliding behavior for accurate friction compensation, IEEE Transactions Automatic Control, 45: 675-686.
[20] Lampaert, V., Al-Bender, F., and Swevers, J., 2003, A generalized Maxwell-slip friction model appropriate for control purposes, IEEE International Conference on Physics and Control Proceedings-PhysCon, St. Petersburg, Russia, pp. 24-31.
[21] Makkar, C., Dixon, W., Sawyer, W.G., and Hu, G., 2005, A new continuously differentiable friction model for control systems design, Proceedings of the 2005 IEEE/ASME International Conference on Advanced Intelligent Mechatronics, Monterey, CA, July 24-28, pp. 600-605.
[22] Jamaludin, Z., Brussel, H. V., Pipeleers, G., and Swevers, J, 2008, Accurate motion control of XY high-speed linear drives using friction model feedforward and cutting forces estimation, CIRP Annals – Manufacturing Technology, 57/1: 403-406.
[23] Schmitz, T., Action, J., Ziegert, J., and Sawyer, W.G., 2005, On the difficulty at measuring low friction: Uncertainty analysis for friction coefficient measurements, Journal of Tribology, 127: 673-678.
[24] Smith S (2000). Flexures: Elements of Elastic Mechanisms. CRC Press, New York, NY.
[25] Schmitz T and Smith KS (2009). Machining Dynamics: Frequency Response to Improved Productivity. Springer, New York, NY.